Alignment strategy for the Inner Detector of ATLAS

P. Brückman de Renstrom[a,b]
for the ATLAS Collaboration

[a] *University of Oxford, DWB, Keble Road, Oxford OX1 3RH, UK*
[b] *Institute of Nuclear Physics PAN, ul. Rdzikowskiego 152, Kraków 31-342, PL*

Abstract
ATLAS is a general-purpose spectrometer in preparation for taking data at the Large Hadron Collider at CERN. It will start operation in autumn 2007. Charged particle tracking is realized by the Inner Detector. The Inner Detector consists of two silicon subsystems: a Pixel Detector and a Semiconductor Tracker complemented by straw proportional gas chambers. In order to exploit the excellent intrinsic resolution of the precision tracking devices high accuracy alignment is required. In this report the strategy to align the sub-detectors of the ATLAS Inner Detector is reviewed, together with the current status of preparation. Both track-based and hardware alignment methods are presented.

16.1 Introduction

The ATLAS Inner Detector (ID) consists of the silicon tracking system closer to the interaction point and a straw-tube gaseous detector system, the Transition Radiation Tracker (TRT), as shown in Fig. 16.1.

The silicon tracking system of the ATLAS ID is composed of two subsystems: the Pixel Detector and the the SemiConductor Tracker (SCT). Altogether it consists of 5832 individual silicon modules which amounts to 34 992 degrees of freedom (DoF)[1]. These are arranged in three Pixel and four SCT cylinders in the barrel part and three Pixel and nine SCT disks in each of the end-caps. 50 μm $\times$ 400 μm pixels provide a 2D readout with 14 μm $\times$ 115 μm resolution, respectively[2]. SCT modules consist of two single-sided back-to-back strip detectors with a relative 40 mrad stereo angle. Barrel SCT modules have parallel strips with 80 μm pitch, while end-cap ones have a fan-out structure. In the barrel the resolution in the direction perpendicular to the strips is 23 μm per side, whilst the stereo angle provides 580 μm resolution along the strips.

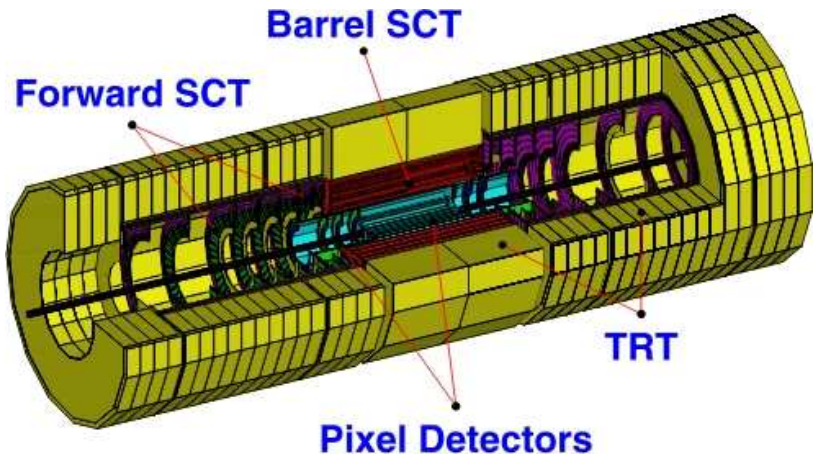

Fig. 16.1: Schematic view of the Inner Detector of ATLAS showing its component subsystems

[1] Each module, assumed to be rigid, has three translational and three rotational DoFs.
[2] Based on single pixel binary readout. This can be further improved [1]

Alignment corrections for silicon are defined in the local reference frames of the modules with $local\ X$ along the sensitive direction[3] and $local\ Y$ being the orthogonal in-plane direction.

The TRT consists of ∼300 000 straw tubes. They have a diameter of 4 mm and provide single measurement resolution of around 150 μm in the direction perpendicular to the wire. TRT straws are arranged into 96 barrel modules and 28 end-cap disks. Degrees of freedom of barrel modules and endcap disks make the basis of TRT alignment parameters.

More details about the Pixel, the SCT, and the TRT systems can be found elsewhere [1, 2].

16.2 The alignment strategy

With the alignment parameters defined in the previous section, the TRT appears to have much fewer degrees of freedom than the silicon system. However, being a drift device, the TRT also needs T0 calibration at a single straw level and determination of the RT[4] dependence with some coarse granularity. Consequently, TRT alignment and calibration represents different challenges to the ones associated with the silicon system. The current strategy assumes an intrinsic alignment of the silicon tracker followed by TRT alignment to the tracks extrapolated from the silicon. An alternative approach integrating the alignment of both the silicon and the TRT in a single algorithm is now undergoing initial validation[5].

The overall strategy for the alignment of the Inner Detector relies on track-based offline alignment algorithms complemented by the Frequency Scanning Interferometry (FSI) system in the SCT. The two have complementary roles as discussed in Section 16.5. The initial alignment of all subsystems is provided by the mechanical and optical surveys of the as-built geometry.

16.3 Track-based alignment algorithms

Three independent algorithms for track-based alignment of the ID silicon detectors complemented by the χ^2-based alignment of the TRT modules have been developed simultaneously. All are based on reconstructed track-to-hit residuals which carry information about track fit quality, and ergo quality of the alignment. All of the methods described have been implemented in the Athena [3] framework and are part of the official ATLAS software.

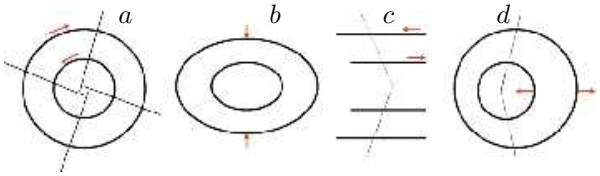

Fig. 16.2: Geometry distortions corresponding to so-called 'weak modes' of the track based alignment: 'clocking' described by $\delta\phi = \beta/R$ (a), various radial distortions (b), 'telescope' described by $\delta Z \sim R$ (c), and ϕ dependent sagitta distortion described by $\delta X = \lambda R + \gamma R^2$ (d). Sagitta can also be η dependent ($\delta\phi = \kappa R\cot(\theta)$) corresponding to a global twist of the barrel, global ($\delta\phi = \gamma R$), and so on. In all cases R denotes the nominal radius of the detector cylinder.

Track-based alignment inherently suffers from so-called 'weak modes' which correspond to detector deformations that do not (significantly) compromise χ^2 of track fits. A few examples of weak mode distortions are shown in Fig. 16.2. The caption gives a brief description of their nature. Such deformations lead to biases on reconstructed track parameters. Notably, all sagitta distortions bias reconstructed track curvature, hence its transverse momentum. Some of these can be eliminated by introducing a common vertex constraint, constraints on track parameters coming from external tracking systems, or direct constraints on the alignment parameters. Cosmic events, representing off-axis continuous helices across the whole detector volume, also provide a powerful tool against some weak modes. Track-based algorithms include implementations of the above mentioned functionalities. For more discussion see Ref. [4].

16.3.1 Real data challenges

Track-based algorithms were applied to two real experimental set-ups. In summer 2004 the Combined Test Beam (CTB) collected the first ever real data from all of the ATLAS subsystems combined [5]. The ID silicon geometry consisted of six Pixel modules and eight SCT ones, followed by six TRT modules all arranged in a tower.

The SCT modules were exactly perpendicular to the beam line, whilst the Pixel modules were arranged with a tilt angle of around 20°. The CTB benefitted from abundant event statistics at different beam momenta[6],

[3] Parallel to the short pixel side and across SCT strips.
[4] Relationship between the drift time and the distance from the anode wire.
[5] TRT is believed to help in constraining track curvature, hence to eliminate notorious sagitta distortions.
[6] 2–180 GeV/c with $O(10^5)$ tracks/module/energy.

whilst a very small set-up and the layout creating ill-defined modes (collimated beam through a narrow tower of modules) were a clear disadvantage. Data were taken with and without magnetic field[7]. Figure 16.3 compares the momentum reconstruction in the simulation with the perfect geometry and the actual detector realigned with different alignment algorithms (described in the following sections). The agreement with simulation is remarkably good. The Robust method is not expected to perform identically since it does not attempt to correct all DoFs.

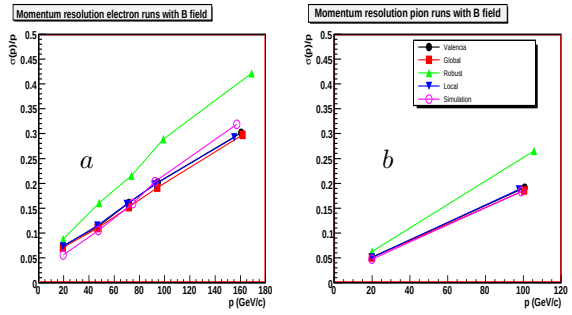

Fig. 16.3: Momentum reconstruction in the CTB electron (a) and pion (b) runs after alignment. Open circles show analogous performance on Monte Carlo with nominal geometry. The data-points labelled 'Valencia' are issue of the dedicated CTB alignment procedure which does not belong to the ATLAS main stream [6].

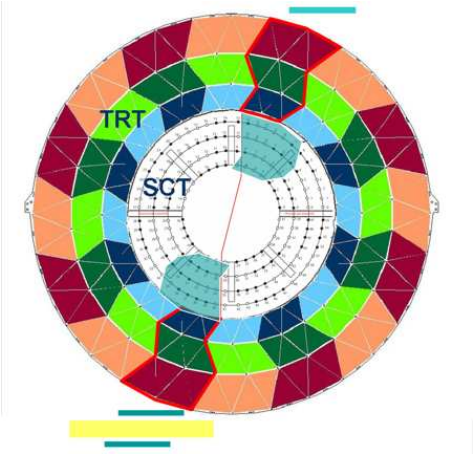

Fig. 16.4: Detector set-up for the 2006 cosmic data-taking in the SR1 building. The regions of SCT and TRT detectors actually read out are indicated. Three scintillator layers working in coincidence provided the trigger for cosmic ray events.

In June 2006 integrated SCT and TRT barrel detectors recorded over 400 000 cosmic events in the ATLAS surface building (SR 1) [7]. The SCT took data with 468 out of 2112 barrel modules in the two opposite wedges of the detector extending over its full length complemented by 12 TRT modules (1/8 of the barrel) as shown in Fig. 16.4. Pixels were not present and there was no magnetic field to reconstruct cosmic ray momenta. Triggering was carried out by three scintillator plates working in coincidence. This challenge involved, for the first time, a larger number of real detector modules in their actual configuration. Lack of magnetic field made momentum reconstruction impossible and the cosmic sample was dominated by very low momentum tracks. Consequently, the tracking error could not be reliably estimated on a track by track basis. Nevertheless, the challenge was an important milestone for both detector operation and the reconstruction tasks.

16.3.2 Robust alignment of silicon detectors

The Robust alignment approach is an iterative method to align any kind of silicon detector with overlapping modules. In each iteration, alignment corrections are calculated out of measurements of mean residuals $\overline{res}$ in the local X and local Y coordinates, and mean overlap residuals $\overline{ovres}$ from overlaps in the local X and local Y coordinates. Local X and Y describe the local axes of the module as defined in Section 16.1. The method aims to correct two to three DoFs only, i.e., two translations in the plane of the module and, if possible, systematic radial translations. The three different residual and overlap residual measurements are combined according to the formula:

$$a_j = -\sum_{j=1}^{3} \frac{s_j}{(\delta s_j)^2} \Big/ \sum_{j=1}^{3} \frac{1}{(\delta s_j)^2}$$

$$s_1 = \overline{res};\;\; s_2 = \sum \overline{ovres}_{LocX};\;\; s_3 = \sum \overline{ovres}_{LocY}\;. \tag{16.1}$$

Alignment corrections (16.1) relate the module position to its adjacent neighbours via local X and Y overlaps. Special care has to be taken in order to propagate corrections across an extended set of modules. The method relies heavily on iteration. More details can be found in Ref. [8].

The method was first validated on the CTB data. It provided fast and stable results. Figure 16.5 shows the improvement to the $local\ X$ residuals in Pixels and SCT due to the alignment. Convergence was always reached within 15 iterations.

The robust method was also applied to the SR 1 cosmic data. Convergence was always reached within ten iterations. Residual distribution in the $local\ X$ direction for SR 1 cosmic tracks after the alignment is shown in Fig. 16.6. The resolution of 35 μm in the peak region can be compared with the analogous figure issued from the Global χ^2 method (32 μm). It turns out to be re-

[7] Magnetic field volume contained only silicon detectors.

markably good given the fact that the robust algorithm exploits only two DoFs per module (the two in-plane translations).

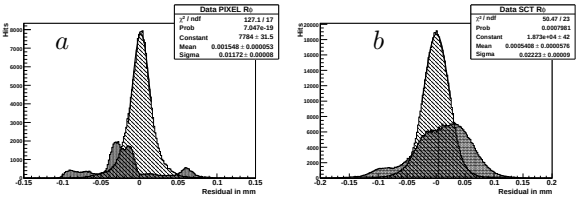

Fig. 16.5: *Local X* residual distributions in CTB Pixel (a) and SCT (b) detectors. Dark-shaded histograms are the initial geometry while the light-shaded ones are after the Robust alignment has converged.

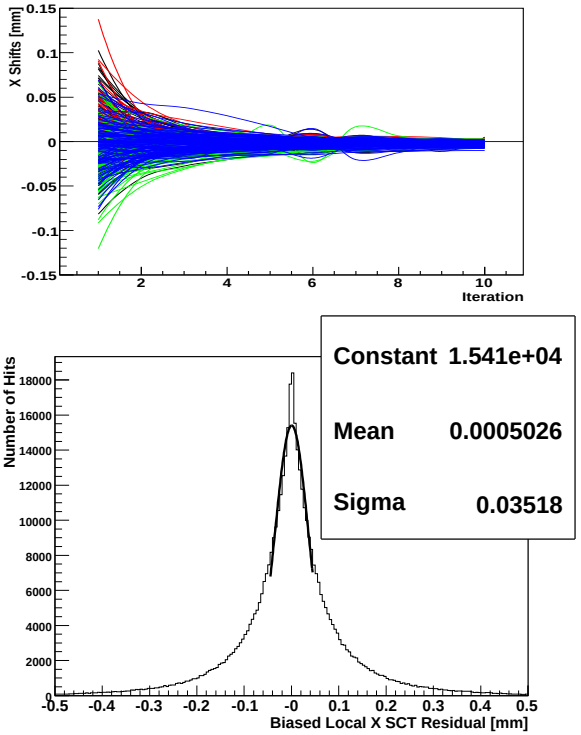

Fig. 16.6: SCT *Local X* residual distributions in SR 1 cosmic events after the Robust Alignment (top). Evolution of the field of alignment corrections in the *local X* direction as a function of iteration number.

The robust alignment algorithm has recently been applied to realign the full geometry of the ID silicon tracking system. The analysis is ongoing but the preliminary results prove the viability of the method.

16.3.3 Global χ^2 alignment of silicon detectors

The Global χ^2 algorithm is based on the minimization of the χ^2 defined as:

$$\chi^2 = \sum_{\text{tracks}} r^T V^{-1} r \tag{16.2}$$

with respect to the alignment parameters. r is the vector of hit residuals to the fitted track and V is its covariance matrix. The residuals depend on the track parameters (π) as well as on the subset of alignment parameters related to the intersected module (a). The sum runs over all reconstructed tracks in the given data sample. The assumption about the corrections being small allows us to use a linear expansion from which the generic solution for the alignment corrections reads:

$$\delta a = -\left(\sum_{\text{tracks}} \frac{dr^T}{da} V^{-1} \frac{dr}{da}\right)^{-1} \sum_{\text{tracks}} \frac{dr^T}{da} V^{-1} r \tag{16.3}$$

with

$$\frac{dr}{da} = \frac{\partial r}{\partial a} + \frac{\partial r}{\partial \pi}\frac{d\pi}{da} \,. \tag{16.4}$$

$d\pi/da$ can be obtained by differentiating the analogous expression for a single track fit to the reconstructed hits in the detector:

$$\delta \pi = -\left(\frac{\partial r^T}{\partial \pi} V^{-1} \frac{\partial r}{\partial \pi}\right)^{-1} \frac{\partial r^T}{\partial \pi} V^{-1} r \,. \tag{16.5}$$

More details about the method can be found elsewhere [9, 10]. The method has a big advantage in that it properly treats all correlations between residuals arising from common track parameters and Coulomb scattering. There is, however, a price to pay. The solution (16.3) requires inverting a symmetric matrix of size N where N is the number of DoFs of the problem. For the ATLAS ID it represents an important numerical challenge. To make things worse, the matrix is inherently singular which requires more careful treatment[8].

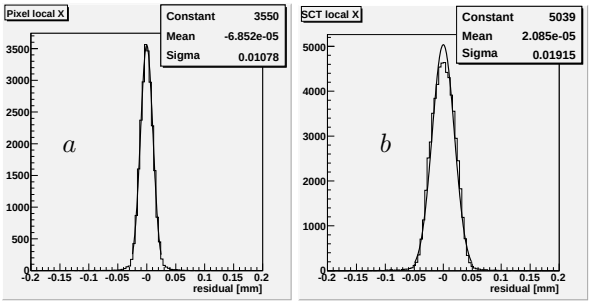

Fig. 16.7: *Local X* residual distributions in the CTB Pixel (a) and SCT (b) detectors resulting from the global χ^2 alignment

[8] E.g. diagonalization. Other options include preconditioning or sequential solving with an arbitrary cut-off. Feasibility of the former was studied and documented elsewhere [11].

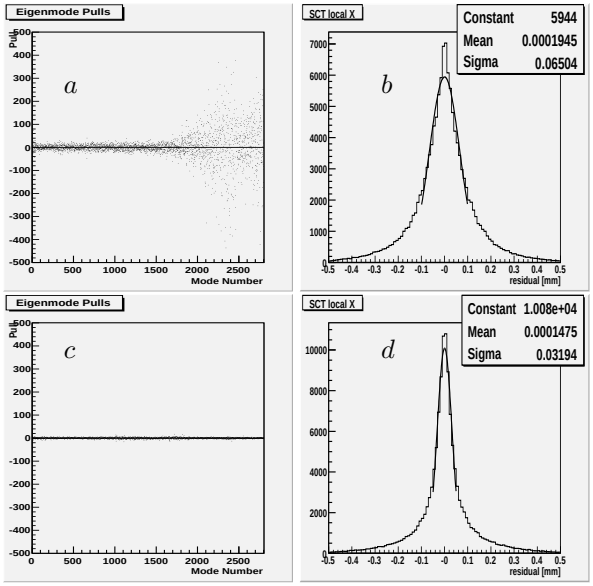

Fig. 16.8: Performance of the global χ^2 algorithm on the SR 1 cosmic set-up (468 SCT modules). The upper plots show the correction pulls for the 2808 eigenmodes (a) and corresponding $local\ X$ residual distribution (b) as obtained from the initial geometry. The lower plots (c and d) show analogous distributions on realigned geometry (after two iterations).

Validation of the global χ^2 algorithm has been carried out on real data from the CTB and SR 1 cosmic runs as well as on fully simulated ATLAS data. For the CTB only two translations and rotation in the module planes were allowed for all modules, whilst the Pixel modules were additionally free to change tilt angle relative to the beam line. This set of parameters exhausted all the relevant DoFs of the system. On the CTB data the method converged within four iterations. Initial broad residual distributions transformed into clean Gaussians with widths of 10.7 μm and 19.1 μm for the Pixel modules and the SCT, respectively, as shown in Fig. 16.7. These were consistent with the perfectly aligned simulation.

Around 250 000 events were used in the analysis of the SR 1 cosmic set-up. Because initial misalignments were small, the convergence was nearly instantaneous. The second iteration already delivered the final quality alignment. The results are summarized in Fig. 16.8. Correction pulls are given in the diagonal base, i.e., the base of orthogonal modes of the detector deformation[9] and are sorted from left to right by increasing eigenvalue. The structure in the right part of plot a shows the misalignment modes that the available data are actually sensitive to. Plot c demonstrates that after the second iteration the alignment fully converged. After alignment the fitted width of the residuals agreed with the one from the perfectly aligned simulation within one micron. The Monte Carlo sample was generated with the actual cosmic muon spectrum cut off at 200 MeV. In real data we had some even lower energy particles. These contributed to the far tails of the residual distribution, but did not affect the width of the peak region. The same data were also used to determine the relative alignment of the four barrels treated as rigid cylinders. In this case, the number of DoFs was reduced to just 6×4 using the following Jacobian transformation of the generic derivatives in (16.3):

$$\frac{dr}{dA_l} = \frac{dr}{da_k}\frac{da_k}{dA_l} \ . \tag{16.6}$$

The Jacobian da_k/dA_l is generally easy to obtain. A denotes the degrees of freedom of the rigid barrels. The results are summarized in Table 16.1.

Table 16.1: Global χ^2 corrections to the rigid SCT barrels from SR 1 cosmic data. Errors are statistical only. The alignment corrections are given in the global ATLAS frame.

	TX [μm]	**TY** [μm]	**TZ** [μm]
Barrel 3	1.9 ± 0.2	-2.3 ± 0.6	-14.6 ± 1.5
Barrel 4	9.2 ± 0.2	41.4 ± 0.5	-38.2 ± 1.4
Barrel 5	7.8 ± 0.2	-9.5 ± 0.5	85.0 ± 1.3
Barrel 6	-18.9 ± 0.2	-29.7 ± 0.6	-32.2 ± 1.4
	RX [μrad]	**RY** [μrad]	**RZ** [μrad]
Barrel 3	3.3 ± 1.7	2.1 ± 0.6	48.9 ± 0.1
Barrel 4	-63.4 ± 1.4	23.8 ± 0.5	52.5 ± 0.1
Barrel 5	45.2 ± 1.4	-15.9 ± 0.5	-93.3 ± 0.1
Barrel 6	26.8 ± 1.6	-8.4 ± 0.6	-8.2 ± 0.1

The algorithm has also been tested on Monte Carlo data simulated through the complete ID geometry. So far, tests have consisted of checking the properties of results obtained on the perfectly aligned detector. Dedicated events containing on average 10 muons with 2 GeV/c < $p_{\rm t}$ <50 GeV/c were used. First, the full barrel part of the Pixel and the SCT detector (21 408 DoFs) was realigned with a limited statistics of 640 000 tracks. The matrix was diagonalized using the `pdsyevd` routine of the ScaLAPACK package on an AMD Opteron parallel cluster [11]. Reconstructed pulls of the alignment corrections exhibited a Gaussian distribution of unit width, as expected. A more recent test benefitted from an ample 7 500 000 tracks simulated into the cone of $|\eta| < 1.0$. The corresponding subset of the Pixel and SCT detectors consisted of 2172 modules (13 032 DoFs). With this high statistic the typical error on the absolute position of the module was of the order of 10 μm. We seem to have observed an over-statistical

[9] These are obtained by means of diagonalization.

fluctuation in one of the low modes corresponding to ϕ rotation of the Pixel detector cylinders relative to the SCT. The corrections to the Pixel modules found by the algorithm are shown in Fig. 16.9. This could indicate a residual systematic effect at some stage of the upstream reconstruction. Fortunately this kind of deformation can be constrained efficiently using a common vertex requirement.

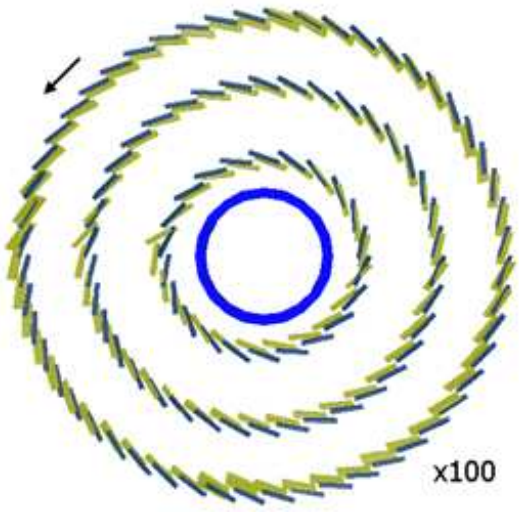

Fig. 16.9: Rotation of the Pixel layers relative to the surrounding SCT as observed in the high statistics attempt to realign 2172 barrel modules using the global χ^2 algorithm. Such a deformation is typical for certain 'weak modes' as discussed in Section 16.3. The nominal module positions in the XY plane are shown in dark blue. The positions after alignment are shown in light green. For visualization purposes distortions have been magnified by a factor of 100.

Large simulated datasets with misaligned ID geometry are currently being analyzed in order to validate full-scale alignment of the distorted ID. The first results using these data are due shortly.

16.3.4 Local χ^2 alignment of silicon detectors

The Local χ^2 algorithm [12] is based on the same ansatz (16.3) but the full derivative (16.4) is reduced to just the partial derivative with respect to a and the full covariance matrix V is replaced by its diagonal only. As a result the system of equations breaks down to 6×6 blocks which are straightforward to solve. The solution is given by:

$$\delta a = -\left(\sum_{\text{tracks}} \frac{\partial r_i^T}{\partial a} \frac{1}{\sigma_i^2} \frac{\partial r_i}{\partial a} \right)^{-1} \sum_{\text{tracks}} \frac{1}{\sigma_i^2} \frac{\partial r_i^T}{\partial a} r_i \ . \tag{16.7}$$

This approximation is justified as long as tracking uncertainty is smaller than measurement uncertainty which is usually a valid assumption. Because all correlations via common track parameters as well as Coulomb scattering are ignored, this method is inherently iterative in order to make up for the reduced information.

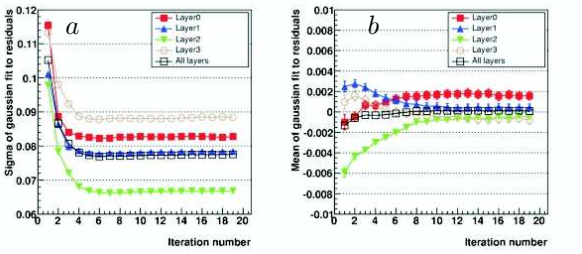

Fig. 16.10: Convergence of the local χ^2 algorithm on the SR 1 cosmic set-up (468 SCT modules). Plots show the widths (a) and the means (b) of the Gaussian fit to the local X residual distributions in the four SCT layers as a function of iteration number (values are given in millimeters).

The local χ^2 method proved its principle providing a good performance on both CTB and SR1 cosmic data. The speed of convergence lies in between the Robust and the Global χ^2 algorithms. For the CTB alignment all DoFs per module were used. The alignment quality after reaching convergence was consistent with the prediction from the perfectly aligned simulation.

On SR 1 cosmic data the algorithm performed the complete alignment procedure involving all six DoFs per module. Figure 16.10 shows the convergence of the algorithm on real SR 1 cosmic data. Full convergence was reached after $\sim$10 iterations. The unbiased hit residual distributions in each SCT layer before and after the alignment are shown in Fig. 16.11. These appear substantially larger than the biased ones used in the Global χ^2 and the Robust methods which is an expected feature [10]. After alignment, the widths are compatible with the perfectly aligned simulation. A similar exercise was performed on the simulation misaligned by as much as the specified assembly tolerances. For the SCT barrel modules were randomly moved in three dimensions within the barrels and the barrels were collectively misplaced with respect to one another. Two main observations were made: the convergence pattern was similar and resulted in comparable track fit quality. The misalignments assumed for the simulation were substantially larger than the ones found in the real system. The latter indicates the excellent precision of the entire SCT assembly.

[10] Unbiased residuals are defined excluding the hit under consideration from the track fit.

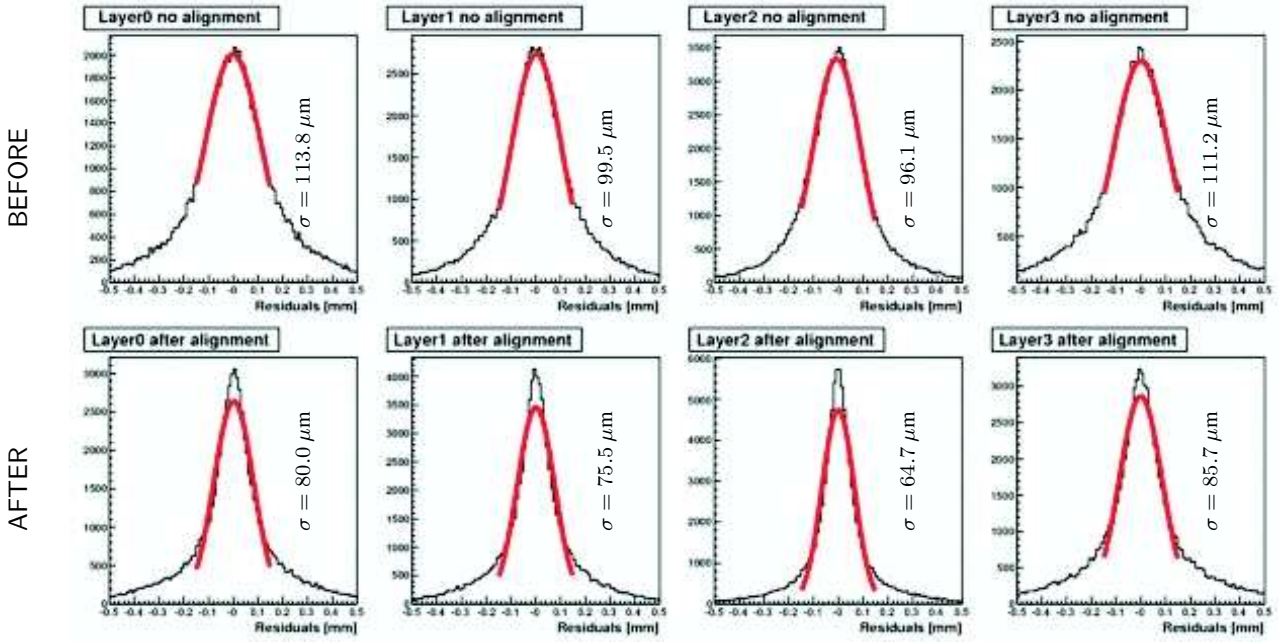

Fig. 16.11: Gaussian fits to the $local\ X$ residual distribution of the SR 1 cosmic tracks before (top) and after (bottom) the Local χ^2 alignment. The fits are made for each SCT layer separately. All residuals are unbiased which make them considerably larger than the biased ones used in the Global χ^2 and the Robust methods.

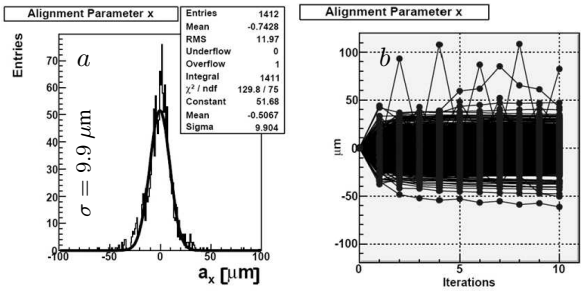

Fig. 16.12: Distribution of the local X corrections to the Pixel modules (a) and the evolution of the individual shift field with iterations (b). Result of the Local χ^2 realignment of Pixel barrel detectors with respect to the SCT in perfectly aligned detector simulation using a limited sample of 100 000 tracks.

The Local χ^2 algorithm was also tried on the full ATLAS geometry using simulated events. At the time of the workshop only a few limited examples were available. One which demonstrates the good stability of the method and adequate error handling is shown in Fig. 16.12. It is based on the perfectly aligned detector. All barrel Pixel modules were realigned relative to the frozen SCT. Corrections in the local X direction have Gaussian distribution and are centred at zero. The corresponding pull distribution is of unit width as expected for correctly estimated error.

The evolution of alignment corrections demonstrates the expected convergence pattern. Only a few outliers show a tendency to oscillate around the optimum[11]. Analysis of the simulation of misaligned full ID geometry is currently underway.

16.3.5 Alignment of the TRT

The current alignment of the TRT is based on the Local χ^2 principle using reference tracks extrapolated from the silicon tracking system (Pixel+SCT). The granularity of the alignment is limited to 96 barrel modules and 28 end-cap disks. Up to five DoFs can be determined for the barrel modules because of the parallel straw assembly whilst for the end-cap disks all six DoFs can, in principle, be reconstructed. As discussed in Section 16.2 the TRT gas chambers need calibration prior to alignment. RT is the relationship between the drift time and the distance from the anode wire and proves to be quite uniform across large sections of the detector. Figure 16.13a shows the RT for all operating TRT modules reconstructed from one SR 1 cosmic run. T0, in turn, can vary substantially within a single TRT module. The worst case from the SR 1 cosmic set-up is shown in Fig. 16.13b. This is why T0 calibration is done on a straw-by-straw basis. Once the calibration is completed the alignment corrections for the TRT modules can be determined.

[11] Most likely edge modules which are less constrained and often suffer from small hit statistics.

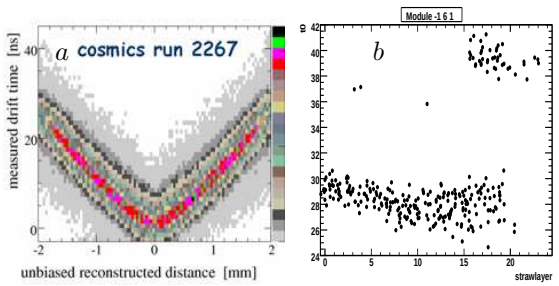

Fig. 16.13: Intrinsic calibration of the TRT drift tubes resulting from the SR 1 cosmic data (run 2267). RT (a) and T0 (b). See text for explanation. Plot b demonstrates clearly why T0 has to be calibrated on a per-straw basis.

During the CTB data-taking the TRT was able to time-dependent monitor and align its position in the direction perpendicular to the straws as well as the dip angle relative to the silicon tracking system. Figure 16.14 shows that the above alignment was extracted with high significance[12].

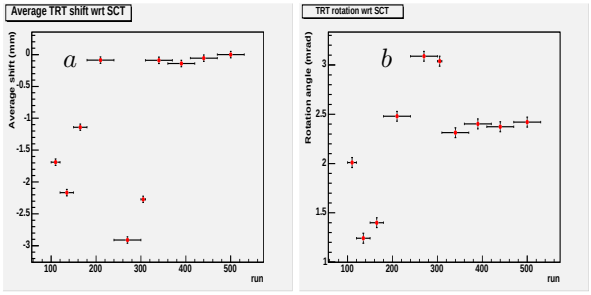

Fig. 16.14: TRT shift in the sensitive direction (a) and rotation (dip angle) (b) relative to the silicon detectors as a function of the run number (time) as reconstructed from the CTB data.

At the time of the Alignment Workshop TRT alignment studies for the SR 1 cosmic set-up were in the preliminary stage. Nevertheless, many useful measurements and observations had been made. Intrinsic residuals for the TRT-only tracks indicated very good assembly precision of the TRT assembly. Matching between track segments from SCT and TRT provided a measure of the global misalignment between the two systems. The results are summarized in Fig. 16.15. A systematic $R\phi$ shift of around 0.5 mm measured at the SCT/TRT boundary was observed, as well as a rotation of about 0.2 mrad in the XZ plane. These preliminary results, however, should be taken with care as the study used track segments from the misaligned SCT detector.

[12] ratio of observed changes to the measurement error

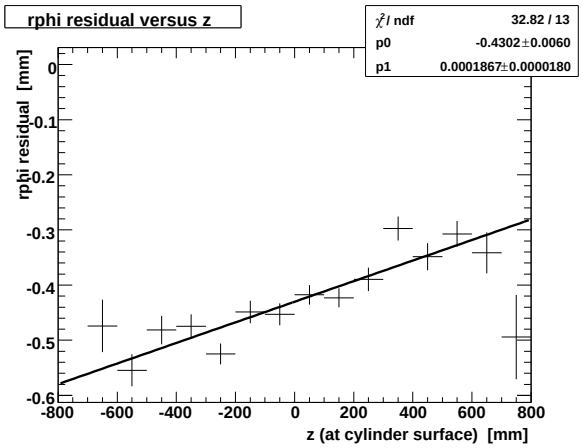

Fig. 16.15: Matching between track segments from the SCT and the TRT in the SR 1 cosmic data at the SCT/TRT boundary. The overall offset indicates an $O(1\ \mathrm{mrad})$ relative ϕ rotation of the two systems. The slope gives evidence of about 0.2 mrad rotation in the XZ plane.

16.4 Survey constraints on alignment

As already mentioned in Section 16.3, track-based alignment methods inherently suffer from lack of sensitivity to certain detector deformations. The latter can lead to biases on reconstructed track parameters. Track alignment can be greatly improved using direct constraints on the detector geometry. These can come from either mechanical or optical surveys of the as-built detector or from the known engineering tolerances and rigidity of the support structures.

Table 16.2: Estimated preliminary uncertainties on the survey alignment parameters for modules on a Pixel barrel stave, modules on a Pixel end-cap sector, modules on an SCT barrel stave, and modules on an SCT end-cap disk [13]. The systematic uncertainties dominate in most cases.

	Pixel stave	Pixel sector	SCT stave	SCT disk
Δx [μm]	50	4.6	150	32
Δy [μm]	20	4.7	150	41
Δz [μm]	50	12.7	150	50
$\Delta\phi_x$ [mrad]	1.7	0.3	2.5	1
$\Delta\phi_y$ [mrad]	5	0.7	5	1
$\Delta\phi_z$ [mrad]	1.7	0.12	2.5	0.09

The estimated preliminary statistical and systematic uncertainties on the local module positions as determined from surveys of the Pixel stave (barrel), Pixel sector (end-cap), SCT stave (barrel), and SCT disk (end-cap) are summarized in Table 16.2. The statistical error

comes from the accuracy of the survey process itself. The systematic uncertainties are mostly related to stability in time and are driven by factors such as mechanical rigidity, moisture, and thermal expansion. The numbers refer to our knowledge of relative module placement within the respective structure and does not represent the total uncertainty on the absolute position in the ATLAS frame. The survey quality was not the same everywhere. Fortunately, in the forward region, where tracking is more challenging due to a larger amount of material and the non-uniform magnetic field, survey data is the most precise.

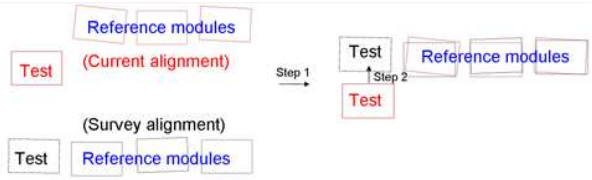

Fig. 16.16: The principle of the 'local constraint' technique. The position of the test module in the current alignment is constrained relative to the reference ones using the corresponding data from the survey [13]

Constraints on the intrinsic geometry of these structures can be accounted for in any generic track-based alignment algorithm using the method described in Ref. [13]. The principle of the 'local constraint' technique is depicted in Fig. 16.16. The leftmost module position can be constrained with respect to the neighbouring ones in two logical steps. First, the reference module positions have to be matched best with the ones defined by the survey. Then, the module to be aligned (test module) can be constrained to the position from the survey within the assumed survey uncertainty.

The most dangerous biases occur from large scale deformations such as sagitta, radial distortions to barrels and global twists. Some of these can be detected for example in the photogrammetric measurements of the assembled detector systems.

Such an attempt was carried out on the complete SCT barrel detector in the SR 1 building prior to the cosmic data-taking [14]. The photogrammetric survey was done before and after inserting the SCT into the TRT. Because of reduced access to the SCT after insertion, the most accurate data were recorded during the first survey. The detector was not guaranteed to have retained the surveyed geometry throughout the process of installation in ATLAS. However, certain characteristics should have been preserved and for the others the engineering model can predict the permitted change. In the first photogrammetry the survey position of eight targets on each of the opposite end flanges of an SCT barrel were measured as shown in Fig. 16.17.

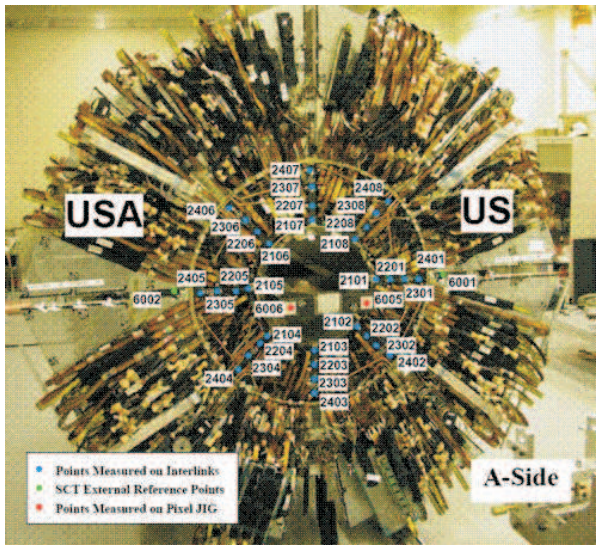

Fig. 16.17: Placement of the photogrammetric targets on side A of the assembled barrel SCT. Side C was equipped identically.

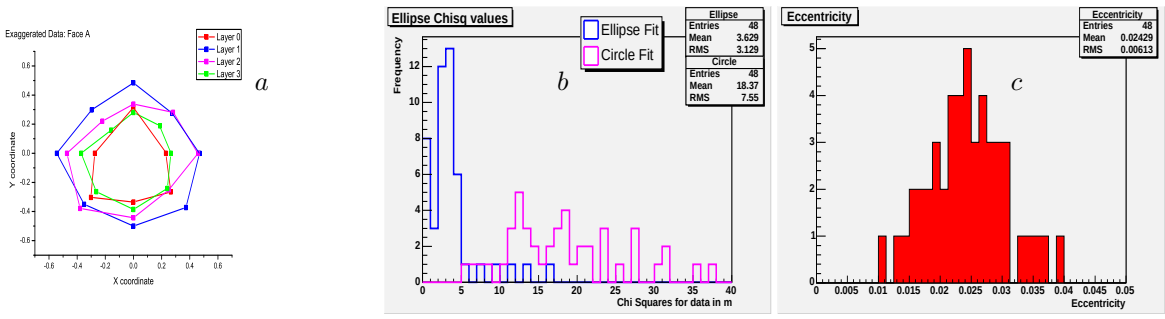

Fig. 16.18: Exagerated displacements of the photogrammetry targets (a), χ^2 values for circular and elliptical fits to the photogrammetry points (b), eccentricity of the fitted ellipses (c). Ellipses are much preferred to circles.

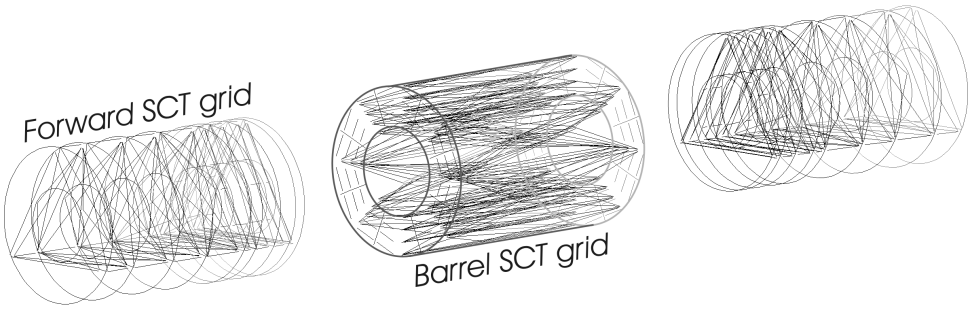

Fig. 16.19: The FSI grid in the SCT. The straight lines represent individual interferometers (842 in total). The circular lines are to guide your eye only.

Altogether, 64 space points were surveyed yielding $O(20\ \mu\mathrm{m})$ precision in the XY plane. After insertion into the TRT only a transfer of the coordinate system was possible, allowing for a crude estimation of the relative SCT and TRT positions. The first survey, however, allowed a more precise analysis of the SCT deformations [15]. Determination of the radial shape of every individual end flange was possible. These were fitted to ellipses yielding orientation of the main axis and and the eccentricity. Figure 16.18a shows the exaggerated deformations as measured on individual barrels of side A. These data allowed various relevant measurements. The radial deformation of individual cylinders was measured by fitting ellipses to the eight respective points. Figure 16.18b shows the histogram comparing χ^2 of the circular and elliptical fits to the measured points in the XY plane. Clearly, the ellipses describe the actual shape much better which indicates a significant departure from the nominal shape. In plot c one can see the histogram of eccentricity of the fitted ellipses defined as $\sqrt{1-B/A}$, with A and B being the minor and major axes of the ellipses, respectively. The values cluster around the value of 0.025 and are inconsistent with zero. The relative ϕ rotations of barrels were also measured. These have a fundamental importance in eliminating the sagitta distortions [4]. By comparing the measurements on phase A and C an indication of an overall global twist was observed.

16.5 Frequency scanning interferometry

FSI is a novel stability monitoring system based on simultaneous measurement of multiple grid line interferometer lengths [16]. The system consists of 842 grid lines arranged into a geodetic grid inside the SCT volume. Grids in the barrel part and the two end-caps are separate, as shown in Fig. 16.19. It also contains a tunable laser and the reference interferometer of precisely known length. Figure 16.20 gives a simple explanation of the principle. Length measurement is based on observing fringes in both the measured and the reference interferometers whilst the tunable laser scans the frequency. The ratio of the observed phase change is equal to the ratio of the interferometer lengths. Node positions can subsequently be reconstructed with an accuracy better than 10 μm in 3D [17].

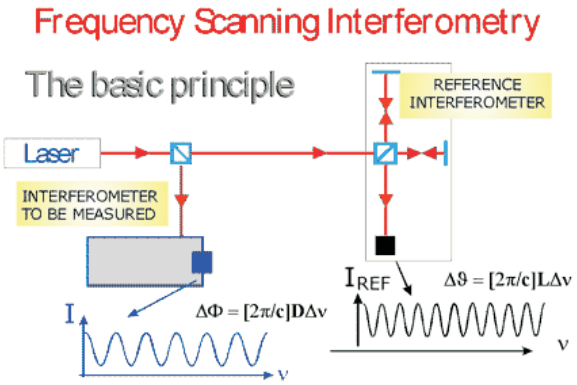

Fig. 16.20: Principle of the length measurement by the Frequency Scanning Interferometer (FSI).

Fig. 16.21: FSI elements mounted on the inner face of an SCT barrel cylinder. The lines show the corresponding grid line interferometers.

The on-detector elements of the interferometers are mounted on the support structures of the SCT, i.e., barrel cylinders (on the inner face) and end-cap disks (on both sides). An example of the barrel FSI elements and corresponding grid lines is given in Fig. 16.21.

The system is capable of monitoring changes to the shape of the SCT mechanical structure. Such time-dependent deformations are expected because of temperature or humidity fluctuations, these driven, for example, by the variable power consumption of the electronics. The FSI provides a quasi real-time (timescale $\sim$10 min) movement field for low spacial frequency eigenmodes which are very difficult to detect with the track-based algorithms. Track alignment, in turn, provides complementary information about high spacial frequency eigenmodes on much longer timescales (24h+). The ideogram of the complementarity of the FSI measurements and the track based alignment is shown in Fig. 16.22.

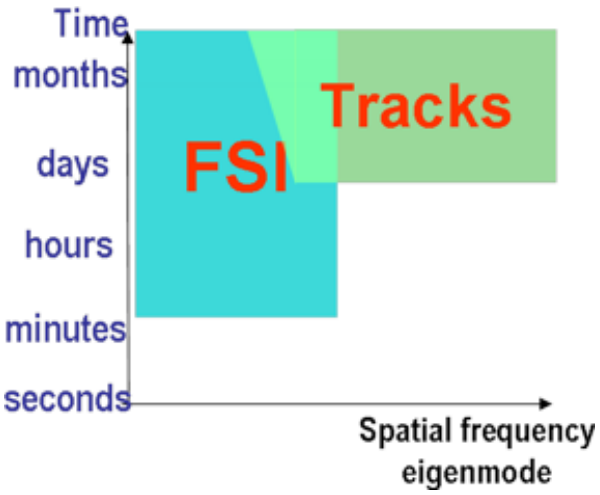

Fig. 16.22: Ideogram showing the time scales and spacial frequency ranges accessible to the FSI and track-based alignment. The two complement each other.

The FSI system will allow corrections to be made to short-term motions of the support structures prior to the offline track alignment.

16.6 Summary and outlook

the ID of ATLAS adopted a variety of techniques in order to ensure optimal alignment of its precision tracking devices. Three independent track-based alignment algorithms to align the Pixel and SCT silicon systems and a complementary algorithm for the TRT are being developed. A novel Frequency Scanning Interferometry system has been integrated into the SCT detector. At all possible construction stages the actual geometry of the as-built detector has been surveyed and the information will be used to impose useful constraints on the offline alignment.

All track-based algorithms have provided convincing proof of principle. Preliminary burn-in of the algorithms was provided by the 2004 CTB. Currently we have started aligning the actual detector. Over 400k cosmic events were collected by integrated SCT and TRT detectors in June 2006. Alignment analysis confirmed that assembly precision outclassed the specified mechanical tolerances.

Large simulation datasets with misaligned geometries of the entire ID are being analyzed now. First alignment results using these data are due soon.

The TRT and SCT barrel parts are already installed inside the ATLAS spectrometer. The FSI is getting ready to monitor SCT distortions. The Pixel detector will be installed in spring 2007. This will be followed by collecting cosmic events in the pit and ultimately by LHC accelerator events due late 2007.

Acknowledgements

We wish to thank O. Buchmüller, P. Coe, M. J. Costa, E. Dobson, M. Elsing, C. Escobar, S. Gibson, T. Golling, G. Gorfine, T. Göttfert, P. Hansen, R. Hawkings, S. Haywood, F. Heinemann, A. Hicheur, D. Hindson, W. Hulsbergen, S. Marti, A. Morley, R. Petti, J. Schieck, S. Sevilla, M. K. Ünel and the entire ATLAS Inner Detector community for their valuable contribution to the topic presented.

References

[1] ATLAS Collaboration, CERN/LHCC 97-16&17 (1997).

[2] ATLAS Collaboration, CERN/LHCC 99-14 (1999).

[3] ATLAS Collaboration, CERN/LHCC 2005-022 (2005).

[4] T. Golling, *Alignment validation*, these proceedings.

[5] B. Di Girolamo, M. Gallas and T. Koffas, EDMS No. 406980 (2005).

[6] ATLAS note in preparation.

[7] `https://uimon.cern.ch/twiki/bin/view/Atlas/InDetCommissioning` .

[8] D. Hindson, DPhil. Thesis, Oxford University (2004);
F. Heinemann, DPhil. Thesis, Oxford University (2007).

[9] P. Brückman de Renstrom, S. Haywood and A. Hicheur, ATL-INDET-PUB-2005-002 (2005).

[10] P. Brückman de Renstrom and S. Haywood, Proceedings of PhyStat05, L. Lyons and

M.K. Ünel (Eds.) (Imperial College Press, London, 2006).

[11] M.K. Ünel, P. Brückman de Renstrom, K. Bernadet and A. Hicheur, CHEP06 proceedings, India (2005).

[12] R. Härtel, Diploma thesis, Technische Universität München (2005), available at http://publications.mppmu.mpg.de/?year=2005&action=search&author=h.rtel&researchfield=&genre=&title=&format=WWW (2005);
T. Göttfert, Diploma thesis, Universität Würzburg (2006), available at http://publications.mppmu.mpg.de/?year=2006&action=search&author=g.ttfert&researchfield=&genre=&title=&format=WWW (2006).

[13] T. Golling, ATL-INDET-PUB-2006-001 (2006).

[14] D. Mergelkuhl and A. Wiart, EDMS No. 681215 (2006);
A. Behrens, V. Correia and J.N. Joux, EDMS No. 705191 (2006);
D. Mergelkuhl and D. Grimm, EDMS No. 708009 (2006).

[15] E. Dobson, ATL-COM-INDET-2007-004 (2007).

[16] P.A. Coe, D.F. Howell and R.B. Nickerson, *Meas. Sci. Technol.* **15** (2004) 2175–2187;
S. Gibson *et al.*, *Opt. Las. Eng.* **43**, Issue 7 (2005) 815–831.

[17] S. Gibson, DPhil. Thesis, Oxford University (2004).